Liu et al. *NPG Asia Materials* (2020) 12:45
https://doi.org/10.1038/s41427-020-0226-7

NPG Asia Materials

ARTICLE Open Access

Control of fibroblast shape in sequentially formed 3D hybrid hydrogels regulates cellular responses to microenvironmental cues

Han Liu[1,2], Mian Wu[1,2], Yuanbo Jia[1,2], Lele Niu[1,2], Guoyou Huang[1,2,3] and Feng Xu[1,2]

Abstract

Cell shape plays important roles in regulating cell behavior; however, independently controlling cell shape in three dimensions is a challenging undertaking, and how cell shape affects cellular responses to mechanical and biochemical cues in three dimensions remains unclear. Here, we present a hydrogel-based platform to control cell shape in three dimensions by using sequentially formed hybrid hydrogels consisting of collagen and alginate. By adjusting the cross-linking time of the alginate, we fixed the shape of NIH 3T3 fibroblasts at different spreading states. Then, we explored the influence of cell shape on the cell responses to microenvironmental cues by using cardiac fibroblasts (CFs) as model cells. We found that the spreading state of the CFs influences their responses to both mechanical (i.e., matrix stiffness) and biochemical (i.e., transforming growth factor-β1 (TGF-β1)) cues in three dimensions. Additional experiments revealed that integrin β1 in focal adhesions and Smad2/3 are involved in mediating the cell shape-dependent responses of CFs to matrix stiffness and TGF-β1 cues, respectively. This work represents the first step in understanding how cell shape influences cell responses to mechanical and biochemical cues in three dimensions and can be instructive for developing novel approaches to target cell shape regulation for treating fibrosis and other diseases.

Introduction

Living cells in vivo reside in a complex three-dimensional (3D) microenvironment composed of multiple biophysical and biochemical cues. Through interaction with the microenvironment, cells adjust their shape to become an integrative repository for signals from multiple sources emerging at different times[1,2]. For example, adipose tissue cells are round, while muscle tissue cells are elongated. These differences in cell shape are interrelated with the tissue morphology and function[3]. Therefore, the shape of cells can indicate their type and function and is affected by the different mechanical and biochemical cues encountered[4]. In addition, an increasing number of studies have revealed that cell shape plays important roles in regulating the growth, migration and differentiation of cells and directing the morphogenesis and functional activities of tissues/organs[1,3,5–7].

Because of typical biological characteristics, such as self-renewal and differentiation capacity, the shape of mesenchymal stem cells (MSCs) has attracted tremendous interest. Researchers have found that cell shape can act as a key regulator in human MSC commitment to adipogenesis or osteogenesis[5,8]. Interestingly, a recent work also reported that the commitment of MSCs is mainly influenced by the generation of degradation-mediated cell traction, not cell morphology or matrix mechanics[9]. In addition to the behavior of MSCs, the behaviors of fibroblasts have been reported to be closely related to cell shape. As one of the major types of stromal cells that are widely distributed throughout the body,

Correspondence: Guoyou Huang (gyhuang@whu.edu.cn) or Feng Xu (fengxu@mail.xjtu.edu.cn)
[1]The Key Laboratory of Biomedical Information Engineering of Ministry of Education, School of Life Science and Technology, Xi'an Jiaotong University, Xi'an 710049, P.R. China
[2]Bioinspired Engineering and Biomechanics Center (BEBC), Xi'an Jiaotong University, Xi'an 710049, P.R. China
Full list of author information is available at the end of the article
These authors contributed equally: Han Liu, Mian Wu

fibroblasts have been demonstrated to be the key effector cells in fibrosis—the leading cause of death worldwide[10,11]. It has been found that, accompanied by abnormal changes in cell microenvironmental cues during fibrosis, the shape of fibroblasts changes[12,13]. In normal tissues, fibroblasts are usually of a spindle-shaped morphology and are retained in a quiescent state with very low secretion and contractile activity. However, under pathological conditions, fibroblasts can differentiate into myofibroblasts by responding to various mechanical and biochemical cues, developing a large and extended morphology with increased secretion and contractile activities[14,15]. Many studies have been conducted to explore the interactions between fibroblasts and the cell microenvironment[16–18]. However, to the best of our knowledge, no report has addressed the role of fibroblast shape on fibroblast responses to microenvironmental mechanical and biochemical cues.

Currently, much of the knowledge acquired to date about the role of cell shape is mainly derived from the development and use of micro-/nanopatterning technologies and hydrogels. Previous studies have developed a series of methods for controlling cell shape on two-dimensional (2D) micro-/nanopatterned substrates[2,8,19]. However, increasing evidence suggests that the behavior of cells in these 2D cultures may be significantly different from that of cells in 3D cultures[20]. Biocompatible hydrogels, including poly(ethylene glycol)[21], hyaluronic acid[22], and alginate[9], have been fabricated with tunable mechanical properties that regulate cell shape in three dimensions. However, some of these hydrogels have a limited ability to regulate cell shape, and some need additional decoration (e.g., RGD peptide) or involvement from additional variables (e.g., changes in stiffness or varying hydrogel degradability). Recently, photocleavable hydrogels[23], 3D micropatterns[1] and microniches[5] have also been developed to engineer cell environments capable of controlling single cell shape in three dimensions or pseudo-three dimensions. However, these techniques may restrict communication between cells and/or can be quite complex. Hybrid hydrogels provide diversified extracellular matrix (ECM)-mimetic elements, in which the adhesion site, mechanical properties and other stimulus signals can be tuned independently[24]. By simply adjusting the sequence of the cross-linking when fabricating hybrid hydrogels, one may be able to independently control cell shape without changing other relative microenvironmental cues.

In this study, we first described the development of a sequentially formed hybrid hydrogel platform and demonstrated its ability to control cell shape in three dimensions. Then, by using cardiac fibroblasts (CFs) as model cells, we investigated the influence of cell shape on the phenotypic transformation of these fibroblasts and found that the spreading state of the fibroblasts has a significant impact on their responses to mechanical and biochemical stimuli. Finally, the underlying mechanism of cell shape-dependent regulation of fibroblast responses to mechanical and biochemical stimuli was explored.

Materials and methods

Sequential formation of collagen–alginate hybrid hydrogels

Type I collagen was extracted from rat tail tendons (the rat tails were from two-month old Sprague-Dawley rats and were supplied by Laboratory Animal Center, Xi'an Jiaotong University School of Medicine), dissolved in 17 mM acetic acid at a concentration of 6 mg ml^{-1} or 10 mg ml^{-1}, sterilized with chloroform, and stored at 4 °C before use. To fabricate the collagen hydrogels, the stored collagen solution was neutralized by immediately pouring 0.2M NaOH onto a prepared polydimethylsiloxane (PDMS; Dow Corning, Midland, USA) mold, allowing the hydrogel to self-assemble at 37 °C for 40 min. To fabricate the collagen–alginate hybrid hydrogels, low molecular weight sodium alginate (Protanal LFR 5/60, kindly supplied by FMC Asia Innovation Center, Shanghai, China) was added at a concentration of 15 mg ml^{-1} to the PDMS mold to cover the self-assembled collagen. This sodium alginate solution was allowed to infiltrate into the collagen for various time intervals, and then, the residual solution was removed and a $CaCl_2$ solution (120 mM) was added to cross-link the alginate that infiltrated into the collagen. To promote the attachment of the collagen hydrogel to the PDMS mold, the surface of the PDMS mold was incubated with 3 μg ml^{-1} collagen solution for 6 h before use. To visualize the distribution of the infiltrated alginate, alginate-fluorescein isothiocyanate was used.

Mechanical characterization

To characterize the mechanical properties of the fabricated hydrogels, hydrogels with a thickness of 2 mm were prepared and soaked in DMEM/F-12 (Corning Cellgro, Manassas, USA) for at least 24 h to allow swelling. After swelling equilibration, hydrogel discs of 15 mm in diameter were prepared using a metal puncher. Rheology measurements were then taken with a rotational rheometer (Anton Paar MCR 302, Austria) using a 15 mm stainless steel parallel plate on a temperature-controlled Peltier system at 37 °C. At the beginning of the test, the plate slowly descended until a normal force of ~50 mN was reached. The exposed edges of the hydrogel samples between the two plates were sealed with mineral oil (Sigma-Aldrich) to minimize dehydration of the samples. The storage modulus and loss modulus were measured by a frequency sweep test performed at a strain of 0.1% and frequency from 0.1 rad s^{-1} to 10 rad s^{-1}. The

corresponding Young's modulus was calculated using the following equation[25],

$$E = 2G(1 + \upsilon) \text{ and } G = \sqrt{G'^2 + G''^2}$$

where E is Young's modulus, υ is the Poisson ratio of the materials (here, we set the value to 0.5), G is the shear modulus, G' is the shear storage modulus, and G'' is the shear loss modulus.

Structural and swelling characterization

To characterize the structure of the collagen, alginate and collagen–alginate hybrid hydrogels, specimens were first fixed in 4% formaldehyde for 1 h, rinsed with DMEM/F-12 for 6 h, sequentially dehydrated in 30%, 50%, 70%, 90%, and 100% ethanol, incubating for 15 min at each gradient step, followed by sequential substitution of ethanol with 30%, 50%, 70%, 90%, and 100% tert-butyl alcohol. Then, the samples were transferred to a freeze-dryer (PowerDry LL1500, Thermo Fisher, USA) to completely remove the solvent. The freeze-dried samples were mounted on a sample stage with double-sided carbon tape and then coated with a thin layer of gold applied by ion sputtering equipment to improve electrical conductivity. The microstructure of the as-prepared specimens was examined using scanning electron microscopy (SEM; ZEISS MERLIN Compact, Germany) at an acceleration voltage of 15 kV.

To characterize the swelling property of the hydrogels, six to ten samples of each hydrogel type (i.e., collagen, alginate, and collagen–alginate hybrid hydrogels) were immersed into sterile DMEM/F-12 for 24 h at room temperature, after which the swollen weight (W_s) of each specimen was recorded. The dry weight (W_d) of each sample was subsequently recorded after freeze-drying. The equilibrium mass swelling ratio was then calculated as W_s/W_d. Based on the results of the mechanical tests and swelling data, it was determined that 3 h was sufficient for alginate infiltration into the collagen networks (2 mm thick). To ensure full penetration of the alginate, all further collagen–alginate hybrid hydrogels (200 μm thick) were prepared using a 60-minute infiltration time.

Cell culture

NIH 3T3 fibroblasts from the Cell Bank of the Chinese Academy of Sciences (Shanghai, China) were used. The cells were cultured in 100% DMEM (Corning Cellgro, Manassas, USA) with 10% fetal bovine serum (FBS; Thermo Scientific, Rockford, USA) and 1% penicillin/streptomycin (Gibco, New York, USA) in a 5% CO_2 humidified incubator at 37 °C.

Primary CFs were isolated as previously reported[26]. In brief, hearts from Sprague-Dawley rats (1–3 days old) were minced and digested with 2 mg ml^{-1} collagenase type II enzyme (MP Biomedicals, Aurora, Ohio) at 37 °C. After centrifugation, the pellets were resuspended in cell culture medium. CFs were preferentially attached to the culture plate after 45 min in a humidified atmosphere with 5% CO_2 at 37 °C. Finally, the isolated CFs were cultured in fresh cell culture medium for further studies. All animal experiments were approved by Xi'an Jiaotong University.

To generate the 3D cell culture, cells were resuspended in DMEM/F-12 medium at a concentration of 10^7 cells ml^{-1} and mixed with neutralized collagen solution (the final concentration of collagen was 3 mg ml^{-1}, and the final concentration of the cells was 5×10^6 cells ml^{-1}). After collagen self-assembly, fresh DMEM/F-12 was added. The cell-encapsulated collagen was incubated for different intervals (i.e., 0 h and 48 h), after which alginate was added and cross-linked as described in "Sequential formation of collagen–alginate hybrid hydrogels". The cells were continuously cultured with the medium being changed once every 2 days.

To test the effect of transforming growth factor-β1 (TGF-β1) on the CFs and to block β1 integrin, 5 ng ml^{-1} TGF-β1 (PeproTech, Rocky Hill, USA) and 1 μg ml^{-1} β1 integrin-blocking antibody (P5D2, Abcam, the UK) were added to the culture medium 2 days after the cells were encapsulated in the respective hydrogel.

Cell staining and image analysis

After cell encapsulation and culture for a different number of days (the time point immediately after encapsulation in collagen was defined as the starting point, i.e., day 0), the cells in the collagen and the cells in the collagen–alginate hybrid hydrogels were subjected to fixation using 4% paraformaldehyde (Sigma) for 15 min, followed by three washes with PBS. Then, the cell membranes were permeabilized with 0.5% Triton X-100 (Sigma) for 15 min and washed three times with PBS. Subsequently, the cells were incubated with 10% normal goat serum (containing 1% bovine serum albumin) for 2 h. The following antibodies were used in the immunofluorescence staining experiments: anti-paxillin antibody (1:200; Abcam, Y113) and anti-vinculin antibody (1:200; Abcam, EPR8185) collectively for focal adhesion staining; anti-Smad2/3 antibody (1:1600; Cell Signaling Technology, 8685) for Smad2/3 staining; Alexa Fluor 488 goat anti-rabbit secondary antibody (1:1000; Thermo Fisher Scientific, A11034) for counterstaining; α-SMA-FITC antibody (1:100; Sigma Aldrich, St. Louis, USA) for α-SMA staining and 4'-6-diamidino-2-phenylindole (DAPI) (Southern Biotechnology Associates, Birmingham, Alabama) and rhodamine phalloidin (1:1000; Thermo Fisher Scientific, R415) for staining of the cell nucleus and cytoskeleton, respectively.

Cell images were captured with a confocal laser scanning microscope (Olympus FV3000, Tokyo, Japan) using ×10, ×40 and ×60 objective lenses. The fluorophores were excited with 405 nm, 488 nm or 561 nm laser lines. To measure the cell-spreading area, the threshold of the cell boundaries was selected manually based on F-actin staining, and the measurement of the spreading area was calculated with ImageJ software (NIH). As the cells described in this paper were cultured under 3D conditions, the spreading area was considered to be represented by the projection of the cells along the z-axis. Focal adhesions were quantified by capturing images of DAPI/phalloidin/paxillin and vinculin antibody-stained cells. The number and length of the focal adhesions were identified manually through color gradation processing, and the background fluorescence intensity from neighboring cell areas was subtracted. The retained stained regions on the cell boundaries were considered representative of the focal adhesions.

mRNA expression analysis

Total RNA extraction was performed on the CFs using a total RNA extraction kit (Tiangen Biotech, Beijing, China) following the manufacturer's instructions. RNA was converted to cDNA using a RevertAid First Strand cDNA Synthesis kit (Thermo Scientific, Rockford, USA) and a thermal cycler (Veriti, Applied Biosystems, Foster City, USA), with the protocol and thermal profile recommended by the manufacturer. A solution containing cDNA, TaqMan gene expression assay reagent (Applied Biosystems, Foster City, USA) and Fast Advanced Master Mix (Applied Biosystems, Foster City, USA) was prepared. A real-time PCR assay was then conducted on a real-time PCR system (Fast 7500, Applied Biosystems, Foster City, USA). The genes analyzed were TGFβR2 (Rn00579682_m1), α-SMA (Rn01759928_g1) and TGF-β1 (Rn00572010_m1). The housekeeping gene used for normalization was GAPDH (Rn99999916_s1). All data are expressed as the fold change in gene expression relative to the group as stated in the figure legends.

Statistics

Statistical analyses were performed using the OriginPro software package (Origin Pro 2016; Origin Lab, Northampton, USA). All data are presented as the means ± standard deviation. Two-sample t-tests were used to determine significance between samples unless otherwise noted. Significance was set at $p < 0.05$ with *, **, and *** indicating $p < 0.05$, 0.01, and 0.001, respectively. NS indicates no significant difference. In addition, $n = 3$ unless otherwise noted. No statistical methods were used to predetermine the sample size.

Results and discussion

Characterization of the sequentially formed collagen–alginate hybrid hydrogels

A schematic of the fabrication of the sequentially formed hybrid hydrogels is shown in Fig. 1a. To ensure that sodium alginate could thoroughly infiltrate into the collagen hydrogels, sodium alginate solutions were maintained in the mold for a sufficient time before being decanted. To characterize the infiltration process of the alginate clearly, we labeled the alginate with FITC and obtained images of the hydrogels at different infiltration times (Fig. 1b). We observed that the alginate uniformly infiltrated into the self-assembled collagen, with the infiltration depth increasing with diffusion time. SEM images revealed that collagen self-assembled to form a typical fibrous structure, while the infiltrated alginate presented as a filler between the collagen fibers, leaving micropores in the hybrid hydrogels (Fig. 1c).

To characterize the influence of the infiltration time of the alginate solution on the mechanical properties of the hybrid hydrogels, self-assembled collagen with a thickness of 2 mm was first fabricated at a concentration of 3 mg ml^{-1}, and then, 15 mg ml^{-1} alginate solution was added and allowed to infiltrate for different lengths of time. The mechanical measurements showed that Young's modulus for the pure 3 mg ml^{-1} collagen hydrogel was 1.17 ± 0.15 kPa. The modulus of the hybrid hydrogel increased with increasing alginate infiltration time, reaching 22.86 ± 0.61 kPa after 3 h of infiltration, after which the modulus did not change significantly even after 6 h of infiltration (Fig. 1d and Fig. S1). In addition, swelling experiments showed that the swelling ratio of the hybrid hydrogel decreased with increasing infiltration time, approaching an unchanged value after 3 h of infiltration (Fig. 1e). These results indicated that 3 h is the saturation time point for alginate infiltration in the collagen network (2 mm thickness). To ensure full penetration of the alginate solution, all additional collagen–alginate hybrid hydrogels (200 μm) were prepared using an infiltration time of 60 min. Moreover, the influences of the collagen concentration and initial alginate concentration on the mechanical properties of the saturated hybrid hydrogels were also investigated. The results showed that Young's modulus of the sequentially formed hybrid hydrogels could be tuned in a wide range, from 23.46 kPa to 130.50 kPa (Fig. 1f, g), indicating that such sequentially formed hybrid hydrogels have extensive adaptability for cell experiments in vitro.

Sequentially formed hybrid hydrogels enable the control of cell shape in three dimensions

To fix cells in different spreading states, sufficient sodium alginate solution was added to the PDMS mold and cross-linked at different times (e.g., day 0 and day 2)

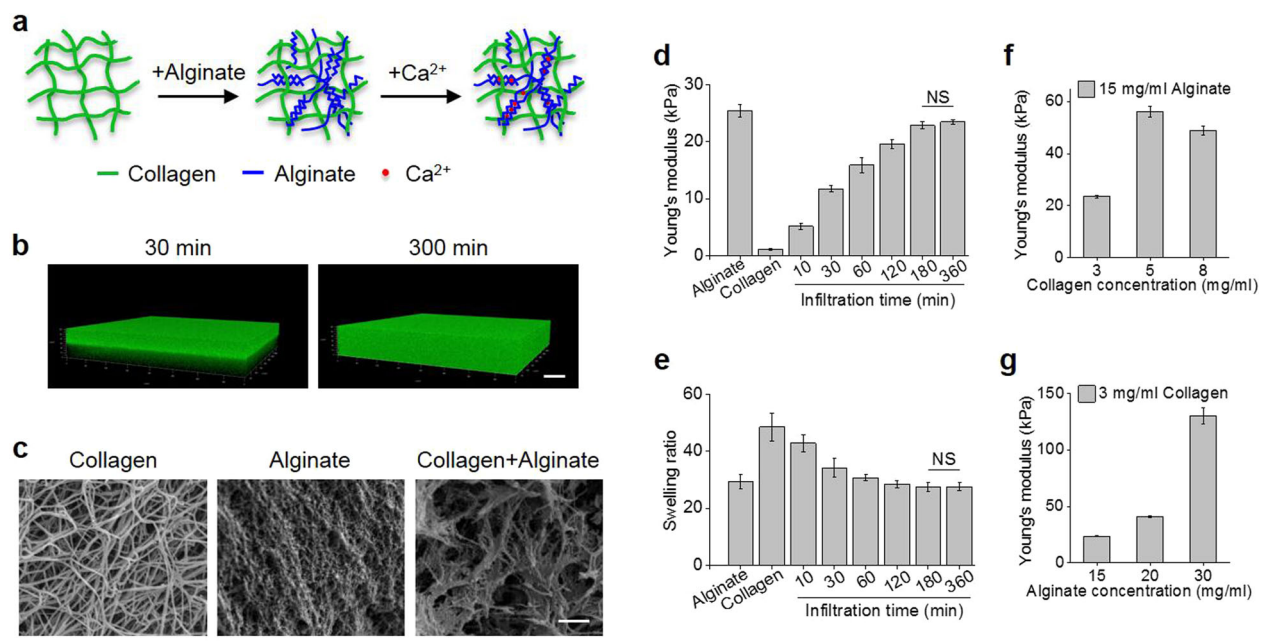

Fig. 1 Schematic and characterization of the sequential formation of collagen–alginate hybrid hydrogels. a Schematic of the sequential formation of collagen–alginate hybrid hydrogels. A collagen solution was first neutralized to allow the self-assembly of the hydrogels at 37 °C. Sodium alginate solution was then added and allowed to infiltrate into the collagen hydrogels. Finally, a calcium chloride solution was added to cross-link the alginate. **b** Representative fluorescence images of FITC-labeled alginate infiltrated into collagen for 30 min (left) and 300 min (right). Scale bar, 50 μm. **c** Representative SEM images of the microstructure of the collagen, alginate and collagen–alginate hybrid hydrogels. Scale bar, 2 μm. **d** Change in Young's modulus of the collagen–alginate hybrid hydrogels with increasing alginate (15 mg ml^{-1}) infiltration times. The collagen concentration was 3 mg ml^{-1}. **e** Mass swelling ratio of the hydrogel shown for the same times recorded in (**d**). **f** Change in Young's modulus of the hybrid hydrogels by collagen concentration with the concentration of alginate fixed at 15 mg ml^{-1}. **g** Change in Young's modulus of the hybrid hydrogels by alginate concentration with the concentration of collagen fixed at 3 mg ml^{-1}.

after cell encapsulation in the collagen. The cells were expected to maintain a round shape even after one week in the hydrogels with alginate added on day 0, and the cells were expected to form a spreading shape in the hydrogels with alginate added on day 2. A schematic of the cell cultures on the collagen–alginate hybrid hydrogels is shown in Fig. 2a.

To investigate cell viability and spreading in the sequentially formed hybrid hydrogels, we first encapsulated NIH 3T3 fibroblasts in 3 mg ml^{-1} collagen and then stiffened the collagen with 15 mg ml^{-1} alginate and 120 mM $CaCl_2$ on day 0 (Col+Alg^{d0} group) or day 2 (Col+Alg^{d2} group). The group with unstiffened collagen and encapsulated cells was denoted as Col (Fig. 2a). We first tested the effects of the hydrogel fabrication process on cell viability. Live/dead staining results indicated that the cells in all groups maintained high cell viability (>95%) after encapsulation, hydrogel stiffening and extended culture for 6 days (Fig. 2b, c), demonstrating that such sequentially formed collagen–alginate hybrid hydrogels were biocompatible and that the cells could thrive regardless of the spreading state.

Next, to examine whether the sequentially formed hybrid hydrogels could control cell shape, we characterized the spreading of the encapsulated NIH 3T3 fibroblasts (Fig. 2d). We observed that the cells in both the Col and Col+Alg^{d2} groups spread extensively after 2 days in culture. From the quantitative analysis results, we found that the spreading area of the NIH 3T3 fibroblasts in the Col group changed from 227 ± 10 μm^2 on day 0 to 757 ± 10 μm^2 on day 6 (Fig. 2e). In contrast, the cells in the Col+Alg^{d0} group were round even after 6 days in culture. Interestingly, in the Col+Alg^{d2} group, the cells maintained a spreading shape after hydrogel stiffening, with no significant change in the spreading area from day 2 to day 6. These results indicate that the sequentially formed collagen–alginate hybrid hydrogels can be used to control cell shape for independent investigation into their roles in cellular responses in three dimensions.

Several studies have shown that cell shape can be regulated in three dimensions by matrix stiffness[9,21,24]. In our study, we fabricated cell-encapsulating hybrid hydrogels by following a sequential formation approach. The steric hindrance of the nonadherent alginate enabled the cells to maintain a round or spreading state at the same 3D matrix stiffness, thus eliminating the influence of matrix stiffness on cell shape[27].

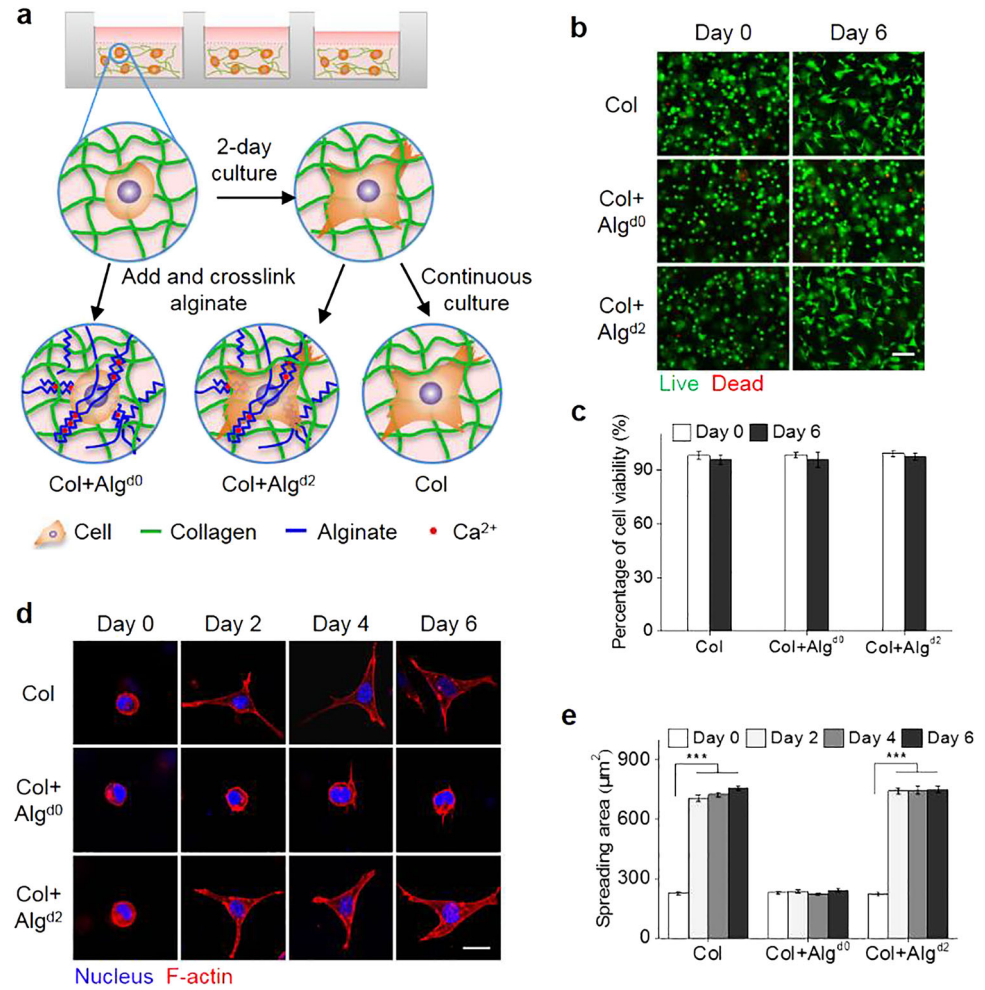

Fig. 2 Sequentially formed hybrid hydrogels enable control of the 3D NIH 3T3 fibroblast shape. a Schematic of the formation of cell-encapsulating collagen–alginate hybrid hydrogels that enable the control of cell shape in three dimensions. **b** Representative live/dead images of cells in the hydrogels immediately after encapsulation (left) and after 6 days in culture (right). Scale bar, 200 μm. **c** Quantity of viable encapsulated cells, calculated as a percentage of live cells among all stained cells. **d** Immunofluorescence-stained encapsulated cells in hydrogels after 0, 2, 4, and 6 days in culture (blue, nucleus; red, F-actin). Scale bar, 20 μm. **e** Spreading area of the encapsulated cells in hydrogels; $n > 50$ cells. * and *** indicate $p < 0.05$ and 0.001, respectively (one-way ANOVA with the Bonferroni post hoc test).

The shape of fibroblasts regulates their responses to matrix stiffness

In cardiac tissue, the differentiation of CFs to myofibroblasts is the main pathological feature of cardiac fibrosis. Along with an increase in the myofibroblast population, collagen secretion increases, resulting in excessive deposition of ECM and adverse remodeling of cardiac tissue, which may ultimately lead to cardiac failure[26]. Recent studies have found that in addition to biochemical cues (e.g., TGF-β1), the mechanical properties of the ECM (e.g., stiffness) have important effects on the differentiation of cardiac myofibroblasts derived from quiescent CFs[28]. Considering that cell shape acts as a key regulator in cell behavior, such as MSC commitment, we speculated that, for CFs, cell shape might play an important role in cellular responses to mechanical and/or biochemical cues.

To explore whether the shape of fibroblasts affects their responses to matrix stiffness, we encapsulated and cultured CFs in hydrogels, similar to the NIH 3T3 fibroblasts. As expected, the CFs in the hydrogels showed controlled spreading behavior similar to that of the NIH 3T3 fibroblasts (Fig. 3a, b and Fig. S2). In addition, the immunofluorescence staining results showed that the CFs in the Col+Alg^{d2} group differentiated into myofibroblasts after 6 days in culture (Fig. 3a). We observed few myofibroblasts in the Col group, although the cells in the Col group had a similar spreading shape as those in the Col+Alg^{d2} group (Fig. 3a, b and Fig. S2). Considering that the stiffness of the hydrogel in the Col+Alg^{d2} group was much

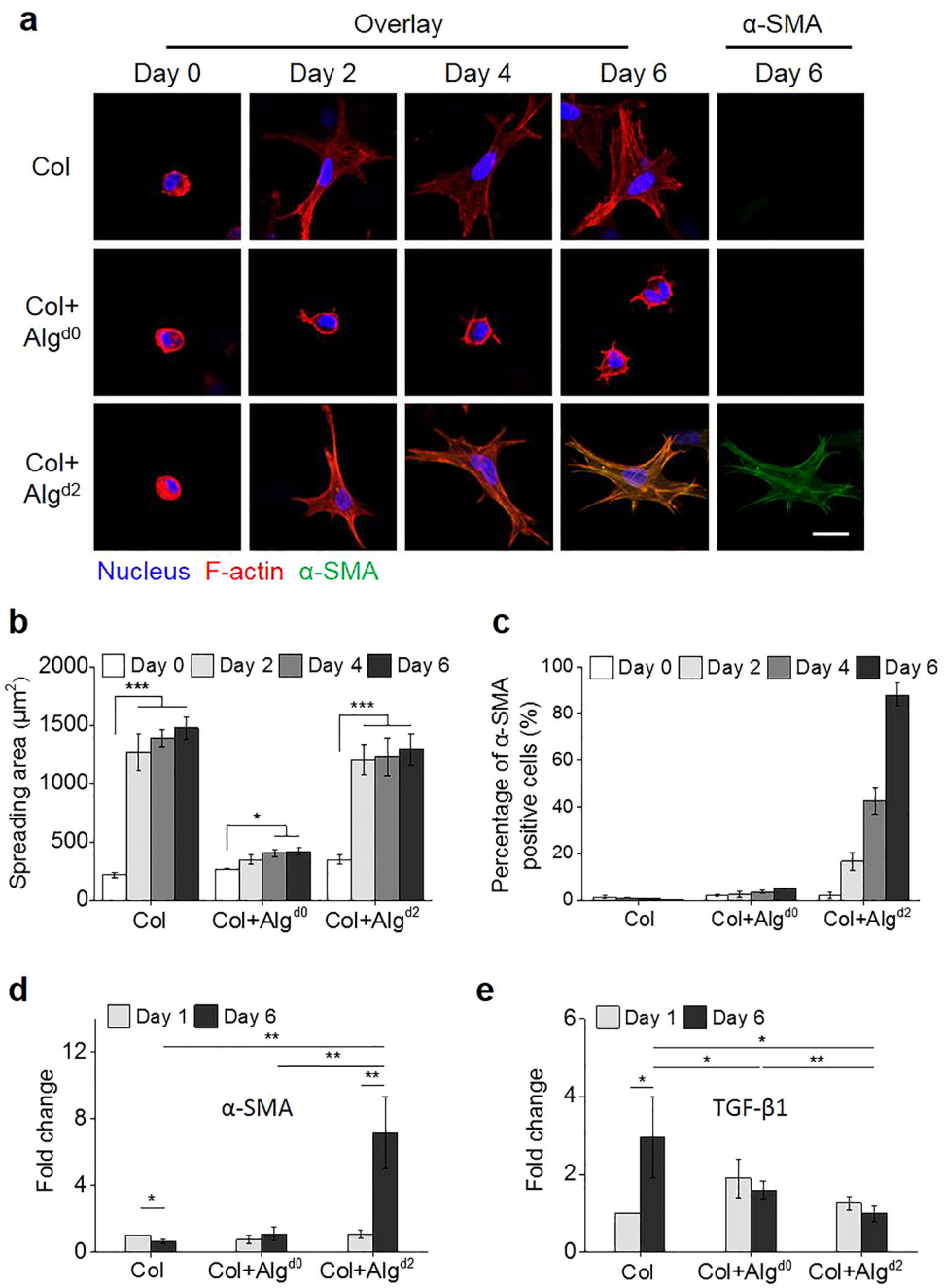

Fig. 3 The shape of the CFs regulates their responses to matrix stiffness. a Immunofluorescence-stained encapsulated CFs in hydrogels after 0, 2, 4, and 6 days in culture (blue, nucleus; red, F-actin; and green, α-SMA). Scale bar, 20 μm. **b** Spreading area of the encapsulated cells in the hydrogels; $n > 60$ cells. * and *** indicate $p < 0.05$ and 0.001, respectively (one-way ANOVA with the Bonferroni post hoc test). **c** Percentage of α-SMA-positive cells in hydrogels; $n > 60$ cells. **d** Results from the quantitative real-time PCR analysis of the gene expression of α-SMA in encapsulated CFs after 1 day and 6 days in culture. **e** Results from the quantitative real-time PCR analysis of TGF-β1 gene expression in the encapsulated CFs after 1 day and 6 days in culture. Fold change was normalized by gene expression levels in the Col group measured on day 1.

greater than that of the Col group, the results indicated that the spreading CFs could sense the 3D matrix stiffness and differentiate into myofibroblasts. Interestingly, the CFs in the Col+Alg^{d0} group showed negligible differentiation behavior, although the stiffness and composition of the hydrogel in the Col+Alg^{d0} group were almost the same as those of the hydrogel in the Col+Alg^{d2} group from day 2 to day 6. The statistical percentage of

α-SMA-positive cells showed that nearly 90% of the cells in the Col+Alg^{d2} group clearly expressed the α-SMA protein on day 6, while only 4.9% and 0.2% of the cells in the Col+Alg^{d0} and Col groups, respectively, were α-SMA positive (Fig. 3c). The results of the gene expression analysis of α-SMA were consistent with the immunofluorescence staining results (Fig. 3d). Taken together and considering the different shapes of the spreading cells in the Col+Alg^{d0} and Col+Alg^{d2} groups, we concluded that cell spreading is necessary for CFs to sense and respond to matrix stiffness in three dimensions.

We further characterized the gene expression of TGF-β1 in the CFs and found that after 6 days in culture, the CFs in the Col group had the highest expression of TGF-β1, while the CFs in the Col+Alg^{d2} group had the lowest expression (Fig. 3e). Since TGF-β1 is a well-known biochemical fibrosis promoter that can be correlated to matrix stiffness, the above results imply that TGF-β1 might not be necessary for CFs to respond to matrix stiffness in our experiments.

To clarify whether the calcium ions (Ca^{2+}) used for sodium alginate cross-linking impact the differentiation of the CFs, we added $CaCl_2$ to the cell culture medium at concentrations of 0, 20 mM and 120 mM (Fig. S3). On the basis of the immunofluorescence staining and quantitative analysis results, we found no difference in α-SMA expression in the three groups described above, indicating that the concentration of Ca^{2+} used in the experiments had no effect on the differentiation of the CFs.

It has been suggested that both cell shape and matrix stiffness can influence cell behavior[2,7], with most of the reported results observed in 2D studies[29]. Here, we provided a simple, sequentially formed hybrid hydrogel platform to independently control cell shape and matrix stiffness to study CF differentiation in three dimensions. As previously documented, CFs respond to increased matrix stiffness by differentiating into myofibroblasts. However, studies have ignored the influence of cell shape on CF differentiation. Our results indicated that cell spreading and rigid matrix stiffness are both necessary for CF differentiation. A recent interesting study found that the differentiation of hMSCs is independent of cell morphology and matrix mechanics but is mediated by cell traction generation through matrix adhesion[22]. The differences in these observations may be due to the use of different materials, a speculation that needs to be further investigated.

The shape of fibroblasts affects their responses to matrix stiffness through focal adhesion regulation

Significant efforts have been made to study cell mechanotransduction[30,31]. Previous studies have demonstrated that cell shape and spreading influence the maturation and distribution of focal adhesions (FAs), which can directly alter the magnitude of cell-exerted contractile forces[32]. We speculated that the shape of the CFs might affect their responses to mechanical stimuli through FAs. To test this hypothesis, the FA complexes in the CFs were stained with immunofluorescence (paxillin and vinculin) in the hydrogels. We observed that mature focal adhesion complexes were mainly found in the Col+Alg^{d2} group and were rarely found in the Col+Alg^{d0} and Col groups (Fig. 4a–c). We also tested the role of integrin β1 (a major component in FAs that mediates the interaction between cells and type I collagen)[33] on cell shape-regulated CF responses to matrix stiffness. From the immunofluorescence staining and gene expression analysis results (Fig. 4d, e), we found that once integrin β1 was blocked, the CFs in the Col+Alg^{d2} group did not differentiate into myofibroblasts, indicating that integrin β1 was required for the spreading CFs to sense and respond to matrix stiffness. Taken together, these findings indicate that the shape of the CFs plays important roles in matrix stiffness-induced phenotype transformation by regulating the formation of mature FAs with integrin β1.

Mature FAs are well known to be primary sensors of mechanical tension[32], and the maturation of FAs is driven by cellular forces from the actin cytoskeleton and/or external forces applied to cells. It has been shown that the areas of high curvature in cells (e.g., cell corners or tentacles) have high traction stress[19], which can enhance the recruitment of integrins to form mature FAs[5]. Previous studies have found that matrix stiffness can affect the size of FAs, while the extent of the cell spreading area can affect the number of FAs formed[34]. We contend that when the CFs are round, the cellular cytoskeletal tension is low and that integrin β1 is not effectively recruited to form mature FAs, thus impairing the ability of CFs to sense and respond to matrix stiffness. The exact mechanism of cell shape-dependent CF mechanotransduction remains to be explored and might be closely related to FA structural proteins (e.g., talin, paxillin, vinculin and tensin)[35].

The shape of fibroblasts regulates their responses to biochemical stimuli

To explore whether cell shape affects the responses of CFs to biochemical stimuli, TGF-β1 was added to the cell culture medium at a concentration of 5 ng ml^{-1} after two days of cell encapsulation. After further culturing for 4 days, immunofluorescence staining and gene expression analysis of α-SMA were conducted. Surprisingly, we observed that the expression of α-SMA increased significantly with the addition of TGF-β1 in the Col and Col+Alg^{d2} groups, while there was no difference in α-SMA expression in the Col+Alg^{d0} group (Fig. 5a, d). In addition, the spreading area and percentage of α-SMA-positive cells did not significantly changed with

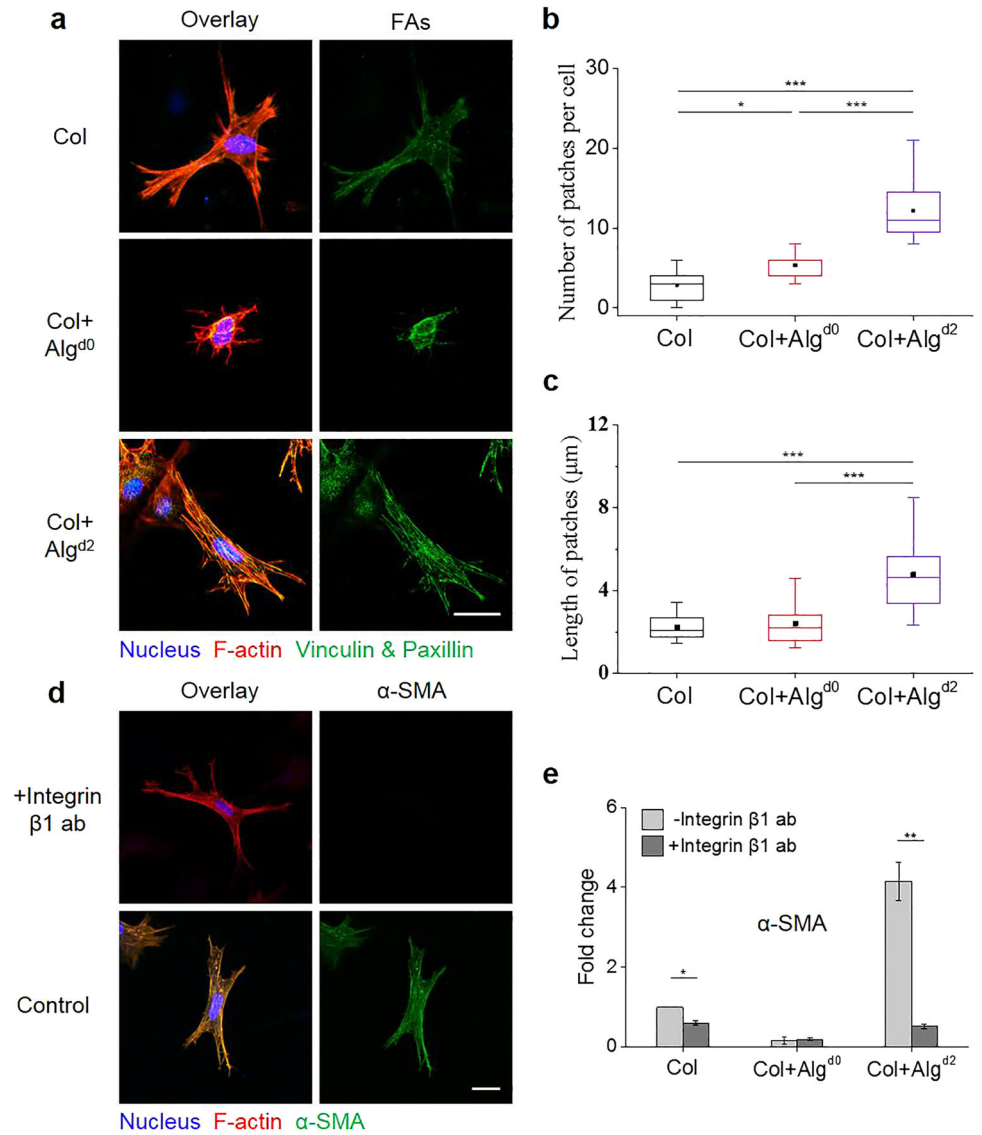

Fig. 4 The shape of the CFs affects their responses to matrix stiffness through focal adhesion regulation. a Immunofluorescence staining of CFs in hydrogels after 6 days in culture (blue, nucleus; red, F-actin; and green, vinculin and paxillin, indicating focal adhesions). Scale bar, 20 μm. **b** Number of focal adhesions per cell. The box plots show the 25/50/75th percentiles, and the whiskers show the 5/95th percentiles. Black dots represent the mean of the data; $n \geq 7$ cells. **c** Quantification of the length of the focal adhesions. The box plots show the 25/50/75th percentiles, and the whiskers show the 5/95th percentiles. Black dots represent the means of the data; $n \geq 23$ adhesions. **d** Immunofluorescence-stained CFs in the Col+Alg^{d2} group after 6 days in culture with or without integrin β1 antibody treatment (blue, nucleus; red, F-actin; and green, α-SMA). Scale bar, 20 μm. **e** Results from the quantitative real-time PCR analysis of the gene expression of α-SMA in the CFs in the Col+Alg^{d2} group after 6 days of culture with or without integrin β1 antibody treatment. The fold change was normalized to the gene expression level measured in the Col group (without integrin β1 antibody treatment).

the addition of TGF-β1 in the Col+Alg^{d0} group (Fig. 5b, c). These results revealed that the shape of the CFs regulated their responses to biochemical stimuli (e.g., TGF-β1).

To further investigate the underlying mechanism of how cell shape influences the responses of CFs to TGF-β1, we first characterized the expression of TGF-β1 receptors in the CFs[36]. Considerable data in the literature have demonstrated that in the classical TGF-β1 signal pathway, TGF-β1 binds and constitutively activates the TGF-β1 type II receptor (TGF-βRII), which in turn recruits and phosphorylates the TGF-β1 type I receptor (TGF-βRI)[37]. From the results of the gene expression analysis of TGF-βRII, we observed that there was no significant difference in TGF-βRII gene expression between the Col+Alg^{d0} and Col+Alg^{d2} groups (Fig. 6a), indicating that the different

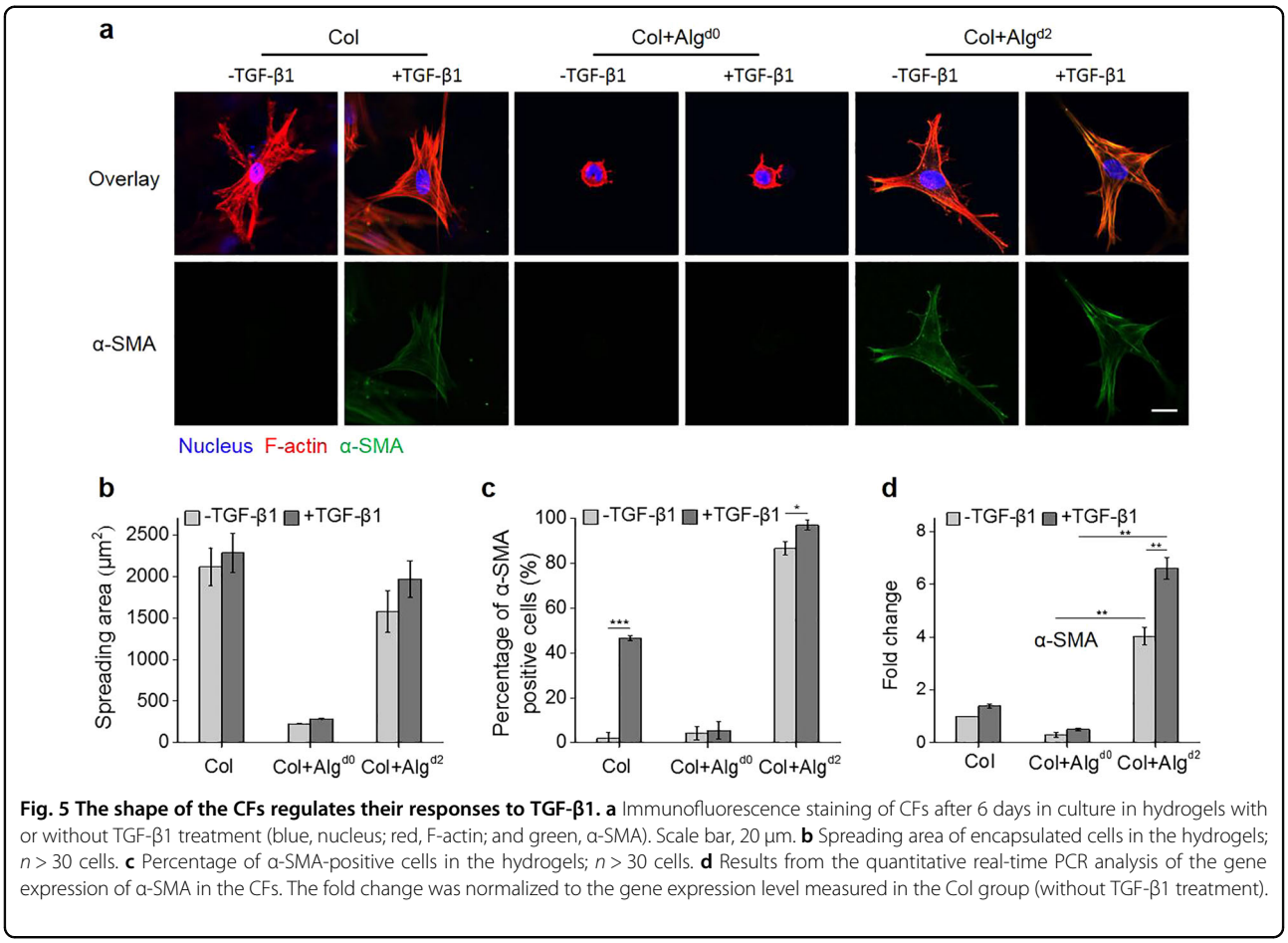

Fig. 5 The shape of the CFs regulates their responses to TGF-β1. a Immunofluorescence staining of CFs after 6 days in culture in hydrogels with or without TGF-β1 treatment (blue, nucleus; red, F-actin; and green, α-SMA). Scale bar, 20 μm. **b** Spreading area of encapsulated cells in the hydrogels; $n > 30$ cells. **c** Percentage of α-SMA-positive cells in the hydrogels; $n > 30$ cells. **d** Results from the quantitative real-time PCR analysis of the gene expression of α-SMA in the CFs. The fold change was normalized to the gene expression level measured in the Col group (without TGF-β1 treatment).

responses of the CFs to TGF-β1 were not induced by the TGF-β1 receptor. Then, we asked whether Smad2/3, downstream of the canonical signal transduction pathway of TGF-β1[38], was the key factor influencing cell responses to TGF-β1. According to the evidence from the immunofluorescence staining and gene expression analysis of Smad2/3, we found that the expression of Smad2/3 was much higher in the Col and Col+Alg^{d2} groups than in the Col+Alg^{d0} group. Moreover, with the addition of TGF-β1, the expression of Smad2/3 increased substantially in the Col and Col+Alg^{d2} groups, but there was only a slight increase in the Col+Alg^{d0} group (Fig. 6b–d). Taken together, these results indicate that the shape of the CFs directed the CF responses to TGF-β1 by regulating Smad2/3 expression.

To date, no direct evidence has shown that TGF-β1 participates in cell shape-mediated mechanotransduction. Some investigations have indicated that antagonism of transient receptor potential vanilloid 4 (TRPV4, a mechanosensitive channel) suppresses TGF-β1-induced activation of Smad2/3[39]. Another TGF-β, i.e., TGF-β3, may interact with integrins to influence the response of chondrocytes to mechanical loading, and TGF-β may induce an increase in the production of integrin receptors[40]. Although we have preliminarily explored the mechanism by which cell shape influences cell responses to TGF-β1, the mechanism remains unclear. Some studies have revealed the influence of the nuclear/cytoplasm ratio of Smad2/3 on CF differentiation; however, we did not observe this trend (Fig. 6e).

Conclusions

In this study, we report a sequentially formed hybrid hydrogel platform consisting of collagen and alginate to control cell shape in three dimensions. We demonstrated that such a hydrogel platform immobilizes the shape of 3T3 fibroblasts according to different spreading states induced by changing the time of adding and cross-linking alginate after cells are encapsulated by collagen. By using CFs as model cells, we found that the spreading state of the cells played a crucial role in regulating their responses to both mechanical (matrix stiffness) and biochemical (TGF-β1) profibrogenic factors. Our study represents a first step in understanding how cell shape influences cell responses to mechanical and biochemical cues. We expect the sequentially formed hybrid hydrogels to be adopted

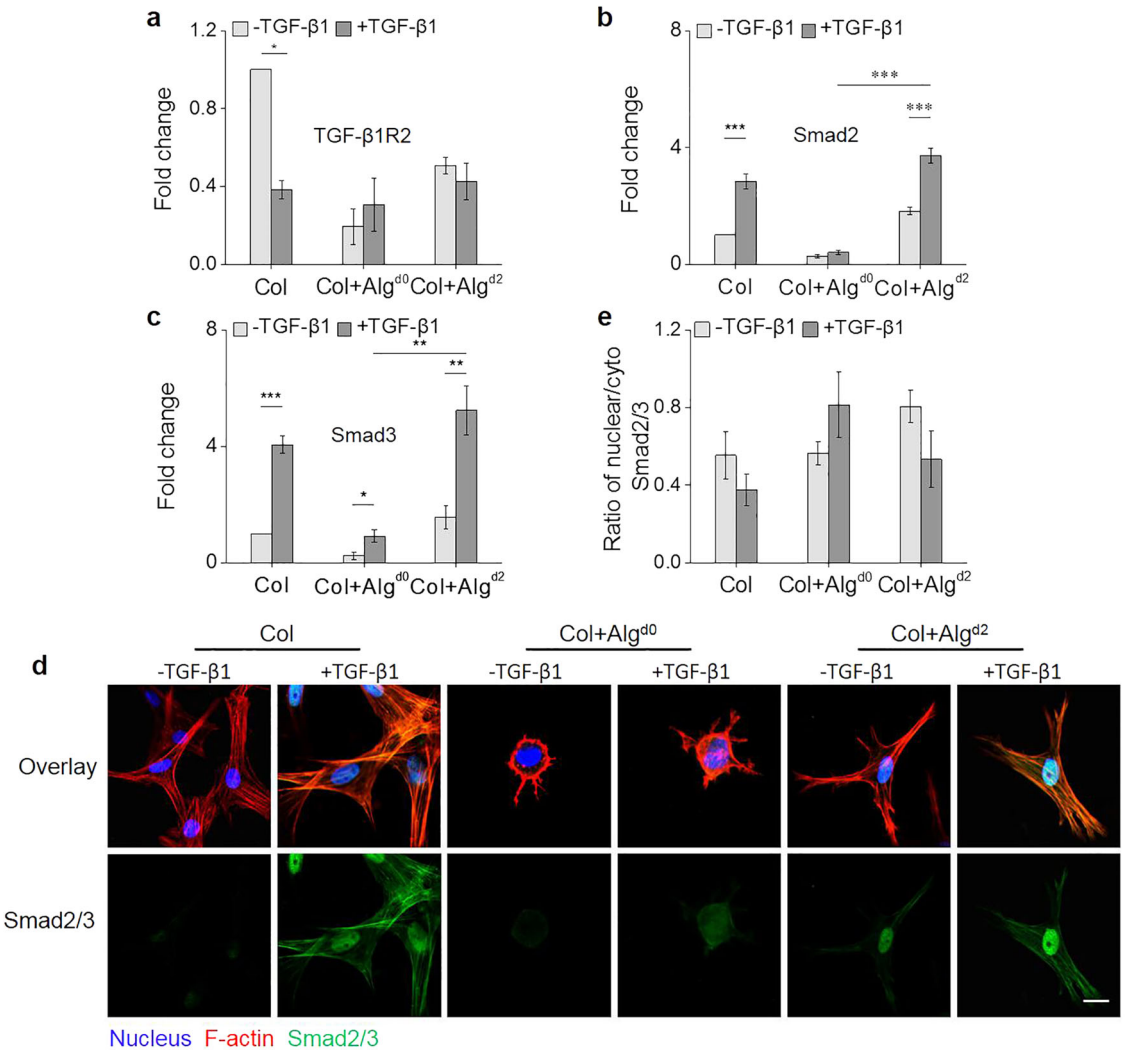

Fig. 6 The shape of the CFs regulates their responses to TGF-β1 through Smad2/3. a–**c**, Results of the quantitative real-time PCR analysis of the gene expression of TGF-β1R2, Smad2 and Smad3 in the CFs. The fold change was normalized to the gene expression level measured in the Col group (without TGF-β1 treatment). **d** Immunofluorescence staining of Smad2/3 in the CFs after 6 days in culture on the hydrogels with or without TGF-β1 treatment (blue, nucleus; red, F-actin; and green, Smad2/3). Scale bar, 20 μm. **e**, Ratio of nuclear Smad2/3 to cytoplasmic Smad2/3.

for investigating many other cell shape-related questions. The results may inspire the development of novel therapeutic approaches for treating fibrosis and other diseases by targeting cell shape regulation.

Acknowledgements
The authors thank Dr. Junjie Zhang for help with the rheology measurements. This study was financially supported by the National Natural Science Foundation of China (11902245, 11872298, 11602191, and 11532009), the China Postdoctoral Science Foundation (2019T120895), and the Fundamental Research Funds for the Central Universities (Z201811336).

Author details
[1]The Key Laboratory of Biomedical Information Engineering of Ministry of Education, School of Life Science and Technology, Xi'an Jiaotong University, Xi'an 710049, P.R. China. [2]Bioinspired Engineering and Biomechanics Center (BEBC), Xi'an Jiaotong University, Xi'an 710049, P.R. China. [3]Department of Engineering Mechanics, School of Civil Engineering, Wuhan University, Wuhan 430072, P.R. China

Conflict of interest
The authors declare that they have no conflict of interest.

Supplementary information is available for this paper at https://doi.org/10.1038/s41427-020-0226-7.

Received: 25 September 2019 Revised: 7 January 2020 Accepted: 26 March 2020.
Published online: 26 June 2020

References

1. Ron, A. et al. Cell shape information is transduced through tension-independent mechanisms. *Nat. Commun.* **8**, 2145 (2017).
2. Chen, C. S., Mrksich, M., Huang, S., Whitesides, G. M. & Ingber, D. E. Geometric control of cell life and death. *Science* **276**, 1425–1428 (1997).
3. Jimenez-Vergara, A. C. et al. Refined assessment of the impact of cell shape on human mesenchymal stem cell differentiation in 3D contexts. *Acta Biomater.* **87**, 166–176 (2019).
4. Prasad, A. & Alizadeh, E. Cell form and function: interpreting and controlling the shape of adherent cells. *Trends Biotechnol.* **37**, 347–357 (2019).
5. Bao, M., Xie, J., Piruska, A. & Huck, W. T. S. 3D microniches reveal the importance of cell size and shape. *Nat. Commun.* **8**, 1962 (2017).
6. Kilian, K. A., Bugarija, B., Lahn, B. T. & Mrksich, M. Geometric cues for directing the differentiation of mesenchymal stem cells. *Proc. Natl Acad. Sci. USA.* **107**, 4872–4877 (2010).
7. von Erlach, T. C. et al. Cell-geometry-dependent changes in plasma membrane order direct stem cell signalling and fate. *Nat. Mater.* **17**, 237–242 (2018).
8. McBeath, R., Pirone, D. M., Nelson, C. M., Bhadriraju, K. & Chen, C. S. Cell Shape, cytoskeletal tension, and rhoa regulate stem cell lineage commitment. *Dev. Cell* **6**, 483–495 (2004).
9. Huebsch, N. et al. Harnessing traction-mediated manipulation of the cell/matrix interface to control stem-cell fate. *Nat. Mater.* **9**, 518–526 (2010).
10. Wynn, T. A. Cellular and molecular mechanisms of fibrosis. *J. Pathol.* **214**, 199–210 (2008).
11. Wynn, T. A. Fibrotic disease and the T(H)1/T(H)2 paradigm. *Nat. Rev. Immunol.* **4**, 583–594 (2004).
12. Bonnans, C., Chou, J. & Werb, Z. Remodelling the extracellular matrix in development and disease. *Nat. Rev. Mol. Cell Biol.* **15**, 786–801 (2014).
13. Rockey, D. C., Bell, P. D. & Hill, J. A. Fibrosis—a common pathway to organ injury and failure. *N. Engl. J. Med.* **372**, 1138–1149 (2015).
14. Thannickal, V. J., Zhou, Y., Gaggar, A. & Duncan, S. R. Fibrosis: ultimate and proximate causes. *J. Clin. Invest.* **124**, 4673–4677 (2014).
15. Zeisberg, M. & Kalluri, R. Cellular mechanisms of tissue fibrosis. 1. Common and organ-specific mechanisms associated with tissue fibrosis. *J. Am. J. Physiol.: Cell Physiol.* **304**, C216–C225 (2013).
16. Kim, D. H. et al. Mechanosensitivity of fibroblast cell shape and movement to anisotropic substratum topography gradients. *Biomaterials* **30**, 5433–5444 (2009).
17. Spinale, F. G. Myocardial matrix remodeling and the matrix metalloproteinases: influence on cardiac form and function. *Physiol. Rev.* **87**, 1285–1342 (2007).
18. Fan, D., Takawale, A., Lee, J. & Kassiri, Z. Cardiac fibroblasts, fibrosis and extracellular matrix remodeling in heart disease. *Fibrog. Tissue Repair* **5**, 15–15 (2012).
19. Oakes, P. W., Banerjee, S., Marchetti, M. C. & Gardel, M. L. Geometry regulates traction stresses in adherent cells. *Biophys. J.* **107**, 825–833 (2014).
20. Huang, G. et al. Functional and biomimetic materials for engineering of the three-dimensional cell microenvironment. *Chem. Rev.* **117**, 12764–12850 (2017).
21. Kloxin, A. M., Kasko, A. M., Salinas, C. N. & Anseth, K. S. Photodegradable hydrogels for dynamic tuning of physical and chemical properties. *Science* **324**, 59–63 (2009).
22. Khetan, S. et al. Degradation-mediated cellular traction directs stem cell fate in covalently crosslinked three-dimensional hydrogels. *Nat. Mater.* **12**, 458–465 (2013).
23. McKinnon, D. D., Brown, T. E., Kyburz, K. A., Kiyotake, E. & Anseth, K. S. Design and characterization of a synthetically accessible, photodegradable hydrogel for user-directed formation of neural networks. *Biomacromolecules* **15**, 2808–2816 (2014).
24. Tong, X. & Yang, F. Engineering interpenetrating network hydrogels as biomimetic cell niche with independently tunable biochemical and mechanical properties. *Biomaterials* **35**, 1807–1815 (2014).
25. Chaudhuri, O. et al. Extracellular matrix stiffness and composition jointly regulate the induction of malignant phenotypes in mammary epithelium. *Nat. Mater.* **13**, 970–978 (2014).
26. Yong, K. W. et al. Paracrine effects of adipose-derived stem cells on matrix stiffness-induced cardiac myofibroblast differentiation via angiotensin II type 1 receptor and Smad7. *Sci. Rep.* **6**, 33067 (2016).
27. Yeh, Y. C. et al. Mechanically dynamic PDMS substrates to investigate changing cell environments. *Biomaterials* **145**, 23–32 (2017).
28. Yong, K. W. et al. Mechanoregulation of cardiac myofibroblast differentiation: implications for cardiac fibrosis and therapy. *Am. J. Physiol.: Heart Circ. Physiol.* **309**, H532–H542 (2015).
29. Yang, Y., Wang, K., Gu, X. & Leong, K. W. Biophysical regulation of cell behavior—cross talk between substrate stiffness and nanotopography. *Engineering* **3**, 36–54 (2017).
30. Chen, C., Li, R. X., Ross, R. S. & Manso, A. M. Integrins and integrin-related proteins in cardiac fibrosis. *J. Mol. Cell. Cardiol.* **93**, 162–174 (2016).
31. Yang, Y. H. & Jiang, H. Y. Cellular volume regulation and substrate stiffness modulate the detachment dynamics of adherent cells. *J. Mech. Phys. Solids* **112**, 594–618 (2018).
32. Chen, C. S., Alonso, J. L., Ostuni, E., Whitesides, G. M. & Ingber, D. E. Cell shape provides global control of focal adhesion assembly. *Biochem. Biophys. Res. Commun.* **307**, 355–361 (2003).
33. Duan, W. et al. The activation of β1-integrin by type I collagen coupling with the Hedgehog pathway promotes the epithelial–mesenchymal transition in pancreatic cancer. *Curr. Cancer Drug Targets* **14**, 446–457 (2014).
34. Han, S. J., Bielawski, K. S., Ting, L. H., Rodriguez, M. L. & Sniadecki, N. J. Decoupling substrate stiffness, spread area, and micropost density: a close spatial relationship between traction forces and focal adhesions. *Biophys. J.* **103**, 640–648 (2012).
35. Stutchbury, B., Atherton, P., Tsang, R., Wang, D.-Y. & Ballestrem, C. Distinct focal adhesion protein modules control different aspects of mechanotransduction. *J. Cell Sci.* **130**, 1612–1624 (2017).
36. Derynck, R. & Zhang, Y. E. Smad-dependent and Smad-independent pathways in TGF-beta family signalling. *Nature* **425**, 577–584 (2003).
37. Guo, Y. J. et al. Entanglement of GSK-3 beta, beta-catenin and TGF-beta 1 signaling network to regulate myocardial fibrosis. *J. Mol. Cell Cardiol.* **110**, 109–120 (2017).
38. van Caam, A. et al. TGF beta 1-induced SMAD2/3 and SMAD1/5 phosphorylation are both ALK5-kinase-dependent in primary chondrocytes and mediated by TAK1 kinase activity. *Arthritis Res. Ther.* **19**, 112 (2017).
39. Sharma, S., Goswami, R. & Rahaman, S. O. The TRPV4-TAZ mechanotransduction signaling axis in matrix stiffness- and TGFβ1-induced epithelial-mesenchymal transition. *Cell. Mol. Bioeng.* **12**, 139–152 (2019).
40. Chowdhury, T. T., Salter, D. M., Bader, D. L. & Lee, D. A. Integrin-mediated mechanotransduction processes in TGFβ-stimulated monolayer-expanded chondrocytes. *Biochem. Biophys. Res. Commun.* **318**, 873–881 (2004).